Bonding Analysis in Inorganic Transition-Metal Cubic Clusters, 5[+] $M_8(\mu_8\text{-}E')(\mu_4\text{-}E)_6L_8$ Species Centered and Hexacapped by Main-Group Atoms

Régis Gautier,[a] François Ogliaro,[a] Jean-François Halet,*[a] Jean-Yves Saillard,*[a] and Evert Jan Baerends[b]

Keywords: Electron count / Electronic structure / Density functional calculations / Transition metals / Cluster compounds / Interstitial element / Main-group elements

The bonding in main-group atom-centered hexacapped transition-metal cubic clusters $M_8(\mu_8\text{-}E')(\mu_4\text{-}E)_6L_8$ has been analyzed by means of density functional theory (DFT) calculations. Although only one example of such compounds has been characterized so far, DFT results indicate that it should be possible for other members of this family to be synthesized. As for their metal-centered parents, there are several "magic" electron numbers that are able to satisfy the closed-shell requirement for such species, depending on the nature of the metal and the capping ligands. The most probable cluster valence electron counts that imply significant M–M bonding are 120 and 122. The former value is favored when E′ is an early main-group element while the latter value is favored when E′ is a late main-group element. Owing to the high connectivity between the atoms, such a regular cubic architecture may also be observed with open-shell electron configurations, as observed for the 119-cluster-valence-electron cluster $Ni_8(\mu_8\text{-}As)(\mu_4\text{-}As)_6(PPh_3)_8$.

Introduction

Among the simplest polyhedral architectures encountered in transition-metal clusters, the M_4 tetrahedral and M_6 octahedral arrangements are by far the most common.[1–4] However, an increasing number of compounds having an M_8 cubic or distorted-cubic cluster core have been characterized in recent years.[5–10] These cubic arrays may be empty[6][7] or centered by an interstitial atom.[8–10] In previous papers, we have analysed the electronic structure of cubic empty clusters of general formula $M_8(\mu_4\text{-}E)_6L_n$ (E = main-group atom or ligand),[11] as well as metal-centered $M_8(\mu_8\text{-}M)(\mu_4\text{-}E)_6L_8$ clusters[12] and other related compounds.[13] These geometries are characterized by a large range of allowed cluster valence electron (CVE) counts, most of which correspond to open-shell configurations or small HOMO–LUMO gaps. The high atom connectivity present in these clusters considerably reduces their Jahn–Teller instability. The largest allowed CVE count generally corresponds to a magic number satisfying the closed-shell requirement for stable diamagnetic molecules.

The possibility of the existence of hexacapped transition-metal cubic clusters centered by a main-group atom has been suggested by Wheeler[14] based on extended Hückel (EH) calculations on $Ni_8(\mu_8\text{-}Te)(\mu_4\text{-}Te)_6L_8$ models, for which he predicted two favored closed-shell CVE counts, namely 110 and 126. On the other hand, the application to these species of Mingos' inclusion principle,[15] which allows prediction of closed-shell electron counts for centered clusters, leads to the values of 114 CVEs and 120 CVEs. More recently, the 119-CVE cluster $Ni_8(\mu_8\text{-}As)(\mu_4\text{-}As)_6(PPh_3)_8$ (**1a**) was synthesized and characterized in the group of D. Fenske.[16] The X-ray molecular structure of this compound (see Figure 1) has exact C_i and approximate O_h symmetries, with the following average bond lengths [Å]: Ni–Ni = 2.89; Ni–(μ_8-As) = 2.50; Ni–(μ_4-As) = 2.32; Ni–P = 2.21; (μ_8-As)···(μ_4-As) = 2.54. This prompted us to undertake a density functional theory (DFT) analysis of the electronic structure of **1a** as well as that of various model clusters of the general type $M_8(\mu_8\text{-}E')(\mu_4\text{-}E)_6L_8$ (E′ = main-group atom; E = main-group atom or ligand) in order to rationalize the bonding, stability and properties of these centered clusters with respect to their possible CVE counts.

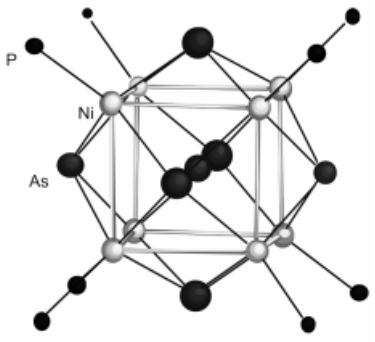

Figure 1. X-ray molecular structure of the 119-CVE cluster $Ni_8(\mu_8\text{-}As)(\mu_4\text{-}As)_6(PPh_3)_8$ (**1a**);[16] the phenyl groups are not shown for the sake of clarity

[+] Part 4: Ref.[13b]

[a] Laboratoire de Chimie du Solide et Inorganique Moléculaire, UMR CNRS 6511,
Université de Rennes 1, F-35042 Rennes Cedex, France
Fax: (internat.) + 33-2/99383487
E-mail: halet@univ-rennes1.fr
[b] Scheikundig Laboratorium der Vrije Universiteit,
De Boelelaan 1083, NL-1081 HV Amsterdam, The Netherlands

  1434–1948/99/0707–1161 $ 17.50+.50/0

Qualitative Approach

The electronic structure of an $M_8(\mu_8\text{-}E')(\mu_4\text{-}E)_6L_8$ compound of approximate O_h symmetry can be qualitatively analysed in a similar way to that previously described by us for the metal-centered $M_8(\mu_8\text{-}M)(\mu_4\text{-}E)_6L_8$ species,[12] i.e. resulting from the interaction of the $M_8(\mu_4\text{-}E)_6L_8$ empty cage with the interstitial atom. We have shown that, as long as there is substantial M−M bonding, a noncentered $M_8(\mu_4\text{-}E)_6L_8$ cube should present a significant HOMO−LUMO gap for the ideal 120-CVE count, separating the more or less nonbonding d-type levels (the d-band) from the significantly antibonding levels.[11] This situation satisfying the closed-shell requirement is represented in the top-middle of Figure 2. The electron configuration corresponding to the 120-CVE magic electron count of the empty cage will be written as $[116](e_g)^4$ in the following discussion.

The interstitial E′ atom has four valence orbitals of a_{1g} (s) and t_{1u} (p) symmetry. They are expected to interact mainly with some metallic counterparts in the d-manifold, which are close in energy and available for bonding. If the four E′ orbitals interact strongly, the resulting antibonding

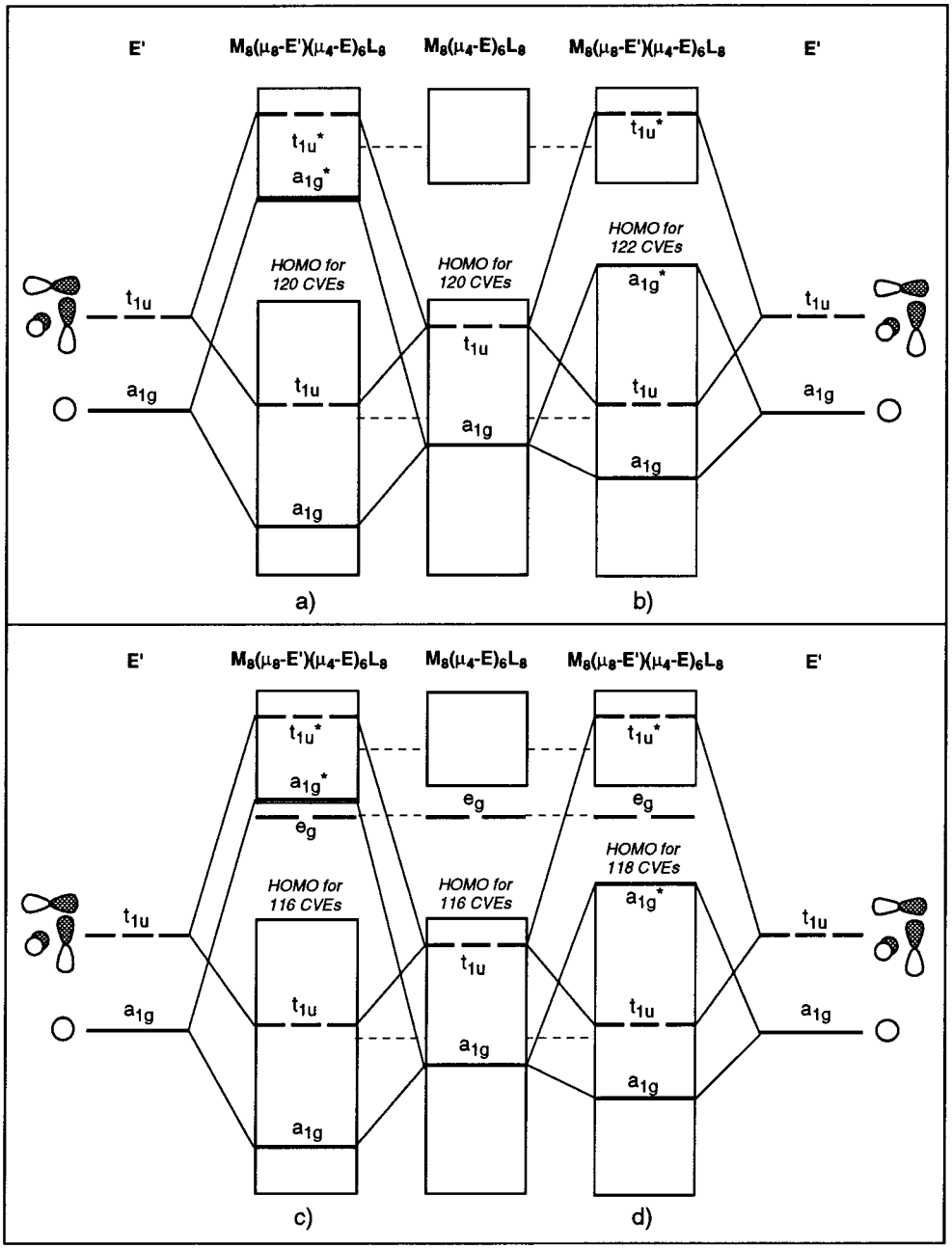

Figure 2. Qualitative MO interaction diagrams for four possible closed-shell configurations in the case of $M_8(\mu_8\text{-}E')(\mu_4\text{-}E)_6L_8$ species in which significant M−M bonding is present: (a) the four s (a_{1g}) and p (t_{1u}) E′ valence AOs interact strongly with the cubic host; (b) only the E′ valence p (t_{1u}) AOs interact significantly; (c) and (d) particular situation where the interactions are similar to those in (a) and (b), respectively, but the capping ligand E is a single main-group atom that tends to destabilize the highest e_g level of the d-band.

combinations will lie at high energy, leaving the same number of bonding and nonbonding levels as in the empty $M_8(\mu_4\text{-}E)_6L_8$, as shown in Figure 2a. In such a situation, the closed-shell requirement is expected to be satisfied for the same 120-CVE count as for the noncentered $M_8(\mu_4\text{-}E)_6L_8$ species, and with the same $[116](e_g)^4$ configuration.

Another closed-shell situation may occur if the E′ atom retains an s-type lone pair, as some heavy main-group atoms often do. This would correspond to a weak a_{1g} interaction, leaving at low energy the weakly antibonding a_{1g} combination. In such a case, a significant HOMO/LUMO gap is expected for the 122-CVE count, corresponding to the $[116](e_g)^4(a_{1g})^2$ configuration. This situation is shown in Figure 2b.

Finally, mention should be made of the special effect induced by the capping E ligands when they are single heavy main-group atoms. This *bare-atom-capping* effect tends to destabilize the highest e_g level of the metallic d-block, whether the cage is centered or not.[12] If this effect is moderate, open-shell configurations will be favored with partial occupation of the e_g level. On the other hand, if this effect is strong enough, the e_g orbitals will become unavailable, leading to the 116-CVE closed-shell count for the empty $M_8(\mu_4\text{-}E)_6L_8$ cluster, with the $[116](e_g)^0$ configuration, as shown in the bottom-middle of Figure 2. In the case of the centered $M_8(\mu_8\text{-}E')(\mu_4\text{-}E)_6L_8$ species, this would correspond to the 116- and 118-CVE possible magic numbers, depending on whether the a_{1g} interaction is strong or not, respectively. These two particular hypothetical closed-shell situations are represented in Figure 2c and d.

The 119-CVE Cluster $Ni_8(\mu_8\text{-}As)(\mu_4\text{-}As)_6(PH_3)_8$

In order to reduce computational effort, cluster **1a** was modeled by changing the PPh_3 ligands into PH_3 phosphanes. Single-point spin-polarized DFT calculations were first performed on $Ni_8(\mu_8\text{-}As)(\mu_4\text{-}As)_6(PH_3)_8$ (**1b**), with an idealized O_h geometry obtained by averaging the experimental structure of **1a** and assuming P−H distances of 1.42 Å. The ground state was found to be a doublet, with the configuration $[116](a_{1g})^2(e_g)^1$. Unfortunately, no experimental data about the magnetic properties have been reported so far for **1a** to confirm this doublet spin state. The level ordering corresponding to spin-restricted calculations is shown in Figure 3. The $5e_g$ and $6a_{1g}$ levels are close in energy and lie in the middle of a large gap separating the nonbonding levels from the antibonding ones. Clearly, the magnitude of the a_{1g} interaction as well as the magnitude of the e_g destabilizing effect due to the bare capping As atoms are both intermediate between strong and weak. The $5e_g$ and $6a_{1g}$ orbitals are plotted in Figure 4. Both are Ni−Ni bonding. The $6a_{1g}$ MO is Ni−(μ_4-As) bonding, whereas the $5e_g$ MO is antibonding along these contacts. As qualitatively predicted (Figure 2), $6a_{1g}$ is Ni−(μ_8-As) antibonding. This orbital is also (μ_8-As)···(μ_4-As) antibonding. The $6a_{1g}$ and $5e_g$ levels are situated in the middle of a large energy gap and so the closed-shell requirement for this kind of cluster should be satisfied for two different electron configurations (among the four predicted above): $[116](a_{1g})^2(e_g)^4$ (122 CVEs) and $[116](a_{1g})^0(e_g)^0$ (116 CVEs).

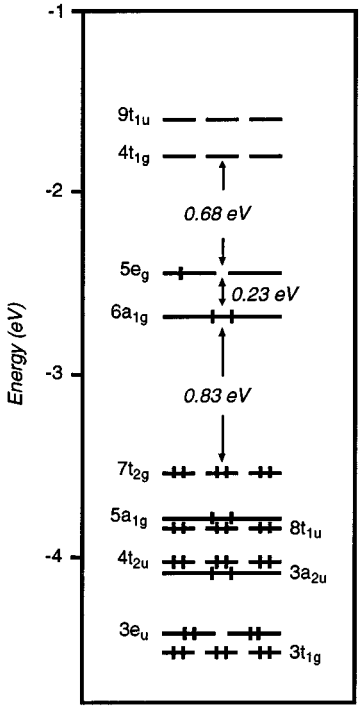

Figure 3. MO level ordering for model **1b** (spin-restricted calculations)

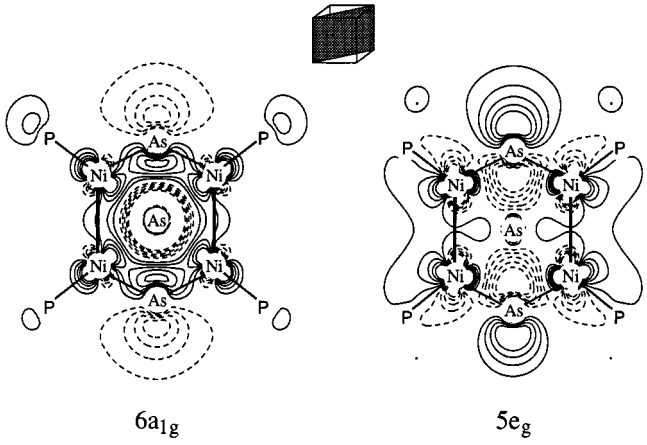

Figure 4. Contour plots of the $6a_{1g}$ and one of the $5e_g$ orbitals of **1b** in one diagonal plane (shaded) containing four Ni atoms and two capping As atoms; contour values are ±0.01, ±0.02, ±0.05, ±0.10, ±0.20, ±0.50 (e $bohr^{-3})^{1/2}$

In a further step, spin-polarized geometry optimizations of **1b** were performed for the three lowest spin states, corresponding to the $[116](a_{1g})^2(e_g)^1$, $[116](a_{1g})^1(e_g)^2$, and $[116](e_g)^3(a_{1g})^0$ configurations, still assuming O_h symmetry. The computed energies and metrical parameters are given in Table 1, together with the data corresponding to the single-point calculations on the averaged experimental structure. The three configurations lead to similar optimized P−H, Ni−(μ_4-As), and Ni−P bond lengths. The latter is in a reasonable agreement with the averaged Ni−PPh_3 exper-

imental value, while the optimized Ni−(μ_4-As) distance is somewhat longer than the averaged experimental one. The Ni−Ni and consequently the Ni−(μ_8-As) separations are found to be strongly dependent upon the electron configuration. Depopulating the $6a_{1g}$ orbital results in decreasing of the size of the cube. This can be attributed to the Ni−(μ_8-As) antibonding character of this orbital. The fact that the Ni−(μ_4-As) distance does not change with the orbital occupations is probably the result of compensating effects associated with the Ni−(μ_4-As) bonding and (μ_8-As)···(μ_4-As) antibonding characters of the a_{1g} orbital.

Other Electron Counts

Geometry optimizations were also performed on model **1b** with different electron counts: 118 CVEs (**1b**$^+$), 120 CVEs (**1b**$^-$), 116 CVEs (**1b**$^{3+}$), and 122 CVEs (**1b**$^{3-}$). The major results are given in Table 1. Again, one can see that the size of the cube strongly depends on the a_{1g} occupation. The other structural parameters primarily vary with the CVE count, almost independently from the electron configuration. It is noteworthy that an increase of the CVE count induces a shortening of the Ni−P distance and an increase of the pyramidalization of the PH_3 ligands. Adding electrons weakens the bonding within the cluster core and reinforces the Ni−PR_3 bonds through π back-bonding. As for **1b**, the three computed electron configurations of **1b**$^+$ and **1b**$^-$ are close in energy, with the lowest state corresponding to an empty $6a_{1g}$ orbital. In this situation, the bonding interaction between the interstitial As atom (considered as neutral) and its cage is maximum. Although significant, the HOMO/LUMO gaps associated with the closed-shell configurations of **1b**$^+$, **1b**$^-$, **1b**$^{3+}$, and **1b**$^{3-}$ are rather small. In order to find examples of clusters having favored CVE counts secured by larger HOMO/LUMO gaps, we have undertaken calculations on different model clusters.

Table 1. Optimized geometries, corresponding HOMO/LUMO gaps and selected bonding energies of cluster **1b** for different cluster valence electron (CVE) counts and electronic configurations

Compound	**1b**$^{3+}$	**1b**$^+$			**1b**			**1b**$^-$			**1b**$^{3-}$
CVE	116	118			119			120			122
Electronic configuration	$(6a_{1g})^0(5e_g)^0$	$(6a_{1g})^2(5e_g)^0$	$(6a_{1g})^1(5e_g)^1$	$(6a_{1g})^0(5e_g)^2$	$(6a_{1g})^2(5e_g)^1$	$(6a_{1g})^1(5e_g)^2$	$(6a_{1g})^0(5e_g)^3$	$(6a_{1g})^2(5e_g)^2$	$(6a_{1g})^1(5e_g)^3$	$(6a_{1g})^0(5e_g)^4$	$(6a_{1g})^2(5e_g)^4$
Ni−Ni [Å]	2.90	3.01	2.91	2.82	2.94	2.86	2.78	2.94	2.87	2.77	2.96
Ni−(μ_8-As) [Å]	2.51	2.61	2.52	2.44	2.55	2.48	2.41	2.55	2.48	2.40	2.56
Ni−(μ_4-As) [Å]	2.47	2.49	2.48	2.49	2.45	2.45	2.45	2.47	2.51	2.47	2.54
(μ_8-As)−(μ_4-As) [Å]	2.83	2.79	2.84	2.89	2.77	2.81	2.85	2.80	2.92	2.88	2.91
Ni−P [Å]	2.36	2.33	2.31	2.30	2.25	2.25	2.26	2.22	2.26	2.24	2.19
P−H [Å]	1.43	1.43	1.43	1.43	1.44	1.43	1.44	1.44	1.45	1.45	1.46
Ni−P−H [°]	119.1	120.9	120.9	120.9	121.8	121.7	121.6	122.7	122.5	122.5	124.1
HOMO/LUMO gap [eV]	0.46	0.44	[a]	[a]	[a]	[a]	[a]	[a]	[a]	0.38	0.63
BE[b] [eV]	−166.72	−185.37	−185.43	−185.61	−190.12	−190.30	−190.37	−192.24	−192.53	−192.77	−188.30
BE_f[c] [eV]	−3.27	−3.44	−3.07	−5.15	−2.23	−2.33	−4.90	−2.25	−4.06	−4.68	−3.53

[a] Open-shell configuration. − [b] Bonding energy with respect to fragmentation in individual neutral atoms. − [c] Bonding energy between the neutral interstitial As atom and its cubic host $Ni_8As_6(PH_3)_8$.

The ADF program allows the calculation of the bonding energy between two or several fragments of a molecule.[19] The bonding energy between the central As atom and its $Ni_8(\mu_4\text{-As})_6(PH_3)_8$ cage in **1b** is given in Table 1 for the three electron configurations considered. Consistent with the Ni−(μ_8-As) and (μ_4-As)−(μ_8-As) antibonding characters of the $6a_{1g}$ orbital, the bonding is stronger when this level is vacant. On the other hand, the depopulation of $6a_{1g}$ to the benefit of $5e_g$ weakens the Ni−Ni and Ni−(μ_4-As) bonding to a similar extent, since the three configurations are close in energy. They lie within a range of 0.25 eV, a value barely significant at the considered level of calculations for such a large cluster. In particular, one should note that the potential energy surface associated with the variation of the Ni−Ni and Ni−(μ_4-As) distances in the O_h symmetry was found to be rather flat. Moreover, **1b** is associated with an open-shell configuration, which may present some Jahn−Teller distortion away from the ideal O_h symmetry. As a matter of fact, the crystal structure of **1a** is of C_i symmetry in the solid state and exhibits some dispersion of the Ni−Ni and Ni−(μ_4-As) separations.[16] Geometry optimizations with lower symmetries, which could allow first-order Jahn−Teller distortion to occur, give results that are not significantly different from those of the $(a_{1g})^2(e_g)^1O_h$ configuration. We therefore conclude that the restriction to the O_h symmetry is a satisfying approximation for analysing the bonding in this type of cluster, owing to their soft flexibility with respect to Ni−Ni distance variation.

Changing the Nature of the Capping and Interstitial Ligands

The 120-CVE and 122-CVE Models $[Ni_8(\mu_8\text{-}E')(\mu_4\text{-}GeH)_6(CO)_8]^{q-}$ (E′ = Si, Ge, P, As, S, Se; $q = 0-4$)

The choice of these hypothetical models was driven by the fact that the diamagnetic 124-CVE metal-centered cluster $Ni_8(\mu_8\text{-Ni})(\mu_4\text{-GeEt})_6(CO)_8$ is known,[8a] and was calculated to present a large HOMO/LUMO gap.[12] Indeed, the presence of Ge−R groups as capping ligands allows to alleviate the destabilizing effect of the cluster e_g frontier level

caused by the μ_4-As bare atoms in **1b**$^{3+/+/-/3-}$. This is expected to particularly favor the 120-CVE and/or 122-CVE magic numbers (see Figure 2a and 2b). In the $[Ni_8(\mu_8\text{-}E')(\mu_4\text{-}GeH)_6(CO)_8]^{q-}$ models (denoted as **[2-E′]**$^{q-}$ in the following discussion), the interstitial main-group atom is varied in order to tune the magnitude of the a_{1g} interaction with respect to the electronegativity and size of E′. The reported calculations correspond to the CVE counts of 120 and 122 for E′ = Si, Ge, P, As, S, and Se. Geometry optimizations have been carried out assuming O_h symmetry. In any case, a single minimum was found on the potential energy hypersurface. The major results are given in Table 2. The computed one-electron level orderings are shown in Figure 5. As expected and in contrast to the case of **1b**, the $5e_g$ level for all the **[2-E′]**$^{q-}$ species lies deep in energy. They are not shown in Figure 5. The highest level of the band occupied for the 120-CVE count is now the $8t_{2g}$ level, which corresponds to the $7t_{2g}$ level in **1b**. In the following discussion the configuration designated above as $[116](e_g)^4$ will be alternatively written as $[110](e_g)^4(t_{2g})^6$. Most of the free anions which were calculated have occupied MOs associated with a positive energy, indicating instability with respect to electron loss. However, when a cationic environment is mimicked by positive point charges introduced in the calculations, these levels are in most of the cases significantly stabilized to negative energies. This is a quite common result for stable anionic clusters.[17] Moreover, it is clear that the hypothetical **[2-E′]**$^{q-}$ clusters should be considered as a series of models for more realistic compounds (see below).

As mentioned above for **1b**, the Ni−Ni separation is very sensitive to the a_{1g} occupation number. In the case of the 120-CVE $[110](e_g)^4(t_{2g})^6(a_{1g})^0$ configuration, this distance lies in the range 2.7−2.9 Å, whereas for the 122-CVE $[110](e_g)^4(t_{2g})^6(a_{1g})^2$ configuration it is longer by ca. 0.2 Å. This difference is smaller in the cases where E′ = S and Se because the a_{1g} level is still occupied in the corresponding 120-CVE configuration. Electron-electron repulsion is also responsible for the long Ni−Ni separations in the negatively charged **[2-E′]**$^{4-}$ (E′ = Si, Ge) and **[2-E′]**$^{3-}$ (E′ = P, As) models. Indeed, the replacement of the CO ligands by isoelectronic NO^+ units in **[2-Ge]**$^{4-}$ leads to shorter optimized Ni−Ni distances in the 122-CVE $[Ni_8(\mu_8\text{-}Ge)(\mu_4\text{-}GeH)_6(NO)_8]^{4+}$ cationic model.

The results on the **[2-E′]**$^{q-}$ series illustrate nicely the trend accompanying the variation of the nature of E′ across the periodic table. When E′ is an early main-group element, the a_{1g} interaction is strong, favoring the closed-shell 120-CVE count. Conversely, with late main-group encapsulated atoms the a_{1g} interaction is weak, favoring the closed-shell 122-CVE count. This is exemplified for the clusters **[2-Si]**$^{2-}$ and **[2-Ge]**$^{2-}$ (120 CVEs), and **[2-S]**$^{4-}$ and **[2-Se]**$^{4-}$ (122 CVEs) for which large HOMO/LUMO gaps are computed.

The 116-CVE and 118-CVE Models: $[Ni_8(\mu_8\text{-}Ge)(\mu_4\text{-}Ge)_6(CO)_8]^{4-}$ and $[Ni_8(\mu_8\text{-}Se)(\mu_4\text{-}Ge)_6(CO)_8]^{4-}$

Starting for example from **[2-Ge]**$^{2-}$ (120 CVEs) and **[2-Se]**$^{4-}$ (122 CVEs), the MO diagrams of which correspond to the general cases of Figure 2a and 2b, the formal removal of the H substituents on the Ge atoms is expected to induce a destabilization of a low-lying e_g level (see above) leading to the general cases of Figure 2c and 2d. In order to check this hypothesis, calculations were carried out on the "deprotonated" models $[Ni_8(\mu_8\text{-}Ge)(\mu_4\text{-}Ge)_6(CO)_8]^{4-}$ (116 CVEs) and $[Ni_8(\mu_8\text{-}Se)(\mu_4\text{-}Ge)_6(CO)_8]^{4-}$ (118 CVEs). They fully confirm the hypothesis illustrated in Figure 2c and 2d, with significant HOMO/LUMO gaps computed for the $[116](eg)^0$ (1.04 eV) and $[116](a_{1g})^2(eg)^0$ (0.88 eV), respectively. As for the **[2-E′]**$^{4-}$ models, the size of the cube is

Table 2. Optimized geometries, HOMO energies and bonding energies for 120-CVE and 122-CVE $[Ni_8(\mu_8\text{-}E')(\mu_4\text{-}GeH)_6(CO)_8]^{q-}$ (**[2-E′]**$^{q-}$) models

E′	Si		Ge		P		As		S		Se	
CVE	120	122	120	122	120	122	120	122	120	122	120	122
Charge ($q-$)	2−	4−	2−	4−	1−	3−	1−	3−	0	2−	0	2−
Ni−Ni [Å]	2.80	3.00	2.87	3.10	2.70	2.89	2.81	2.99	2.75	2.82	2.85	2.94
Ni−E′ [Å]	2.43	2.60	2.49	2.68	2.34	2.50	2.43	2.59	2.38	2.45	2.47	2.54
Ni−Ge [Å]	2.42	2.51	2.46	2.55	2.42	2.48	2.46	2.51	2.44	2.46	2.48	2.50
E′−Ge [Å]	2.80	2.83	2.83	2.84	2.83	2.84	2.85	2.85	2.84	2.84	2.87	2.85
Ge−H [Å]	1.59	1.66	1.59	1.66	1.57	1.62	1.57	1.62	1.56	1.60	1.56	1.60
Ni−C [Å]	1.82	1.80	1.82	1.80	1.83	1.83	1.82	1.80	1.81	1.82	1.81	1.82
C−O [Å]	1.17	1.19	1.17	1.19	1.16	1.18	1.16	1.18	1.16	1.17	1.16	1.17
HOMO energy [eV]	0.86	7.24	0.90	6.51	−1.96	4.21	−2.04	3.78	−5.20	0.87	−5.22	0.76
BE[a] [eV]	−212.37	−202.41	−209.73	−200.70	−211.09	−208.24	−208.74	−206.56	−204.53	−209.15	−202.93	−207.62

[a] Bonding energy with respect to fragmentation in individual neutral atoms.

Closed-shell ground-state configurations, namely $[116](e_g)^4(a_{1g})^0$ {or $[110](e_g)^4(t_{2g})^6(a_{1g})^0$} and $[116](e_g)^4(a_{1g})^2$ {or $[110](e_g)^4(t_{2g})^6(a_{1g})^2$}, were found for all the 120-CVE and 122-CVE models, respectively, except two of them. In the case of the 120-CVE species having E′ = S and Se, the $[110](e_g)^4(a_{1g})^2(t_{2g})^4$ open-shell ground-state configuration was found. This result suggests that with the more electronegative chalcogen elements as encapsulated atoms, the a_{1g} interaction is weak, requiring its occupation even for the 120-CVE count, for which a partially depopulated t_{2g} HOMO is preferred.

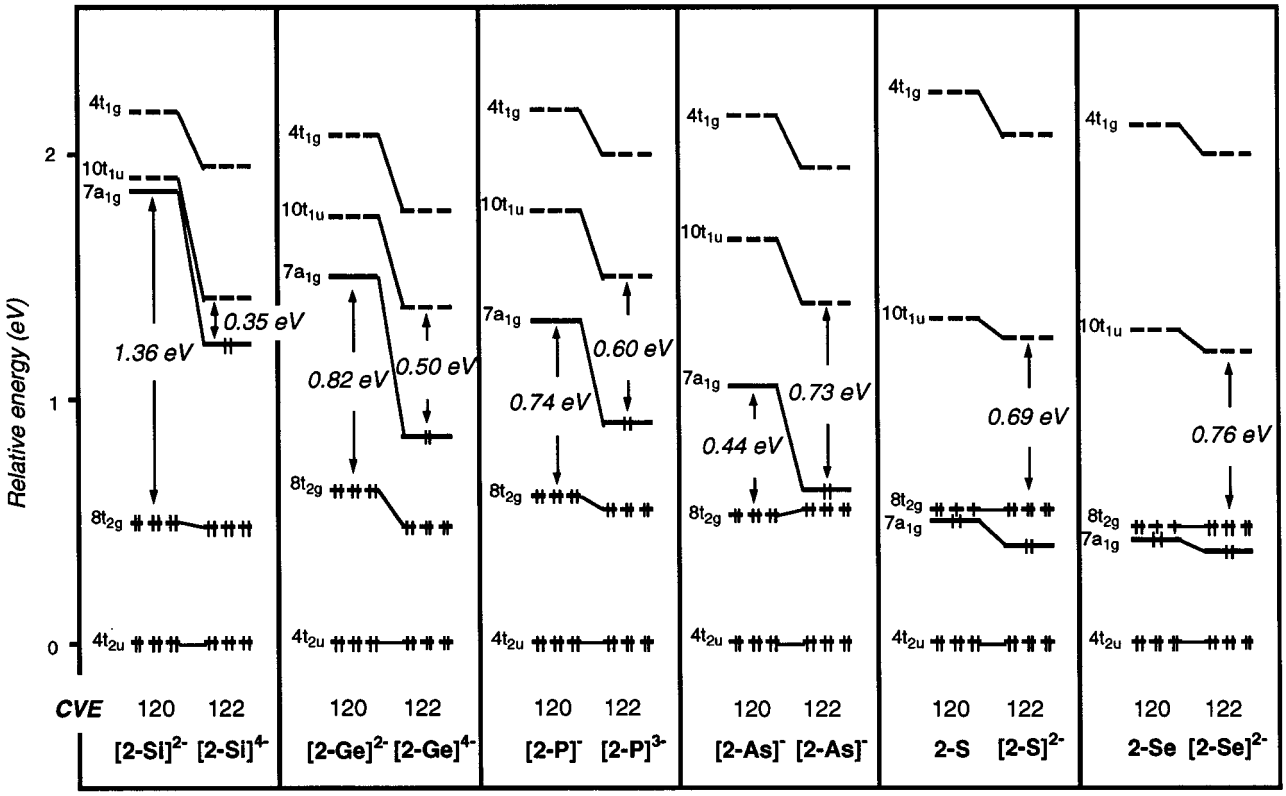

Figure 5. MO level orderings for the 120-CVE and 122-CVE cluster models **[2-E′]**$^{q-}$ (in all cases, the zero energy has been arbitrarily set to be the energy of the $4t_{2u}$ level)

rather large in these highly charged anions (Ni−Ni ca. 3.1 Å). Calculations on the isoelectronic cation $[Ni_8(\mu_8\text{-Ge})(\mu_4\text{-Ge})_6(NO)_8]^{4+}$ (116 CVEs) lead to a similar electronic configuration, with a HOMO/LUMO gap of 1.07 eV. In this latter model, the optimized Ni−Ni and Ni−(μ_4-Ge) distances are 2.79 Å and 2.42 Å, respectively.

Other Possible Electron Counts

The MO diagrams of **[2-E′]**$^{2-/4-}$ (E′ = Si, Ge) and of **[2-E′]**$^{-/3-}$ (E′ = P, As) exhibit a significant gap below the occupied $8t_{2g}$ level. This suggests that the count of 114 CVEs could be a possible closed-shell electron count for some members of the $M_8(\mu_8\text{-E}')(\mu_4\text{-E})_6L_8$ series. This is confirmed by calculations on the $[Co_8(\mu_8\text{-P})(PH)_6(CO)_8]^{3+}$ model (see Table 3), which show a significant HOMO/LUMO gap of 0.60 eV for the $[110](e_g)^4(t_{2g})^0$ ground-state configuration. The $8t_{2g}$ orbitals are mainly localized on the Co atoms (64%) with a very weak participation of the d-type polarization function of the encapsulated atom (its s and p valence orbitals do not have the proper t_{2g} symmetry). They exhibit some Co−Co and Co−(μ_4-P) antibonding character. The monoccupation of these MOs in $[Co_8(\mu_8\text{-P})(PH)_6(CO)_8]^{3+}$ tends to reinforce the corresponding bonds, as illustrated by comparing the corresponding bond lengths with their homologs in the 120-CVE **[2-P]**$^-$ cluster (see Table 2).

Table 3. Optimized geometries and corresponding bonding energies for the 114-CVE $[Co_8(\mu_8\text{-P})(\mu_4\text{-PH})_6(CO)_8]^{3+}$ and the 128-CVE $[Cu_8(\mu_8\text{-S})(\mu_4\text{-GeH})_6(CO)_8]$ species

Model compound	$[Co_8(\mu_8\text{-P})(\mu_4\text{-PH})_6(CO)_8]^{3+}$	$Cu_8(\mu_8\text{-S})(\mu_4\text{-GeH})_6(CO)_8$
CVE	114	128
M−M [Å]	2.68	2.88
M−(μ_8-E) [Å]	2.32	2.50
M−(μ_4-E′) [Å]	2.33	2.59
(μ_8-E)−(μ_4-E′) [Å]	2.69	3.04
P/Ge−H [Å]	1.44	1.60
M−C [Å]	1.87	1.91
C−O [Å]	1.15	1.15
BE_f[a] [eV]	−5.25	−3.80

[a] Bonding energy between the neutral interstitial E′ atom and its cubic host $M_8(\mu_4\text{-E})_6(CO)_8$.

On the other hand, the MO diagrams of **[2-E′]** and **[2-E′]**$^{2-}$ (E′ = S, Se) exhibit large $10t_{1u}/4t_{1g}$ separations, suggesting that the $[110](e_g)^4(a_{1g})^2(t_{2g})^6(t_{1u})^6$ configuration should satisfy the closed-shell requirement in the case of electron-rich metals. This is confirmed by calculations on the 128-CVE $Cu_8(\mu_8\text{-S})(GeH)_6(CO)_8$ model (see Table 3). The optimized Cu−Cu and Cu−Ge distances are long, indicating weak bonding. The $10t_{1u}$ orbitals are predominantly localized on the Cu (28%) and Ge (31%) atoms, with

a smaller S (18%) participation. Although it exhibits some Cu−S antibonding character, this level cannot be identified as being the t_{1u}* level shown in the diagrams of Figure 2. In fact, this $10t_{1u}$ level is better described as being associated with the Cu−Ge bonds.[11] Therefore, its occupation is expected to weaken these bonds (see above) or to induce a Jahn−Teller distortion of the octahedral architecture. Such a distortion is unlikely to occur, as shown by geometry optimizations carried out under the T_d and D_{4h} symmetry constraints, which provide results not significantly different from those obtained under the O_h symmetry.

One may be tempted to compare the 128-CVE face-capped $Cu_8(\mu_8\text{-}S)(GeH)_6(CO)_8$ model and a series of Cu_8 edge-capped cubic 128-CVE clusters synthesized by Fackler, Coucouvanis and co-workers[7] in which the Cu−Cu separations (2.8−2.9 Å) are similar to that optimized in $Cu_8(\mu_8\text{-}S)(GeH)_6(CO)_8$ (2.88 Å). The similarity is, in fact, fortuitous. In the edge-capped clusters the bonding can be simply described by a 2-electron/2-center bonding scheme in which the Cu atoms are 16-electron centers, with no formal Cu−Cu bonding.[5][7] Such a description does not apply at all for the highly delocalized $Cu_8(\mu_8\text{-}S)(GeH)_6(CO)_8$ system. There is also no simple relationship between this latter cluster and the recently characterized edge-capped Cu_8 clusters centered by other main-group atoms.[10]

The 122-CVE count is likely to be the upper limit of the allowed CVE range, since adding more electrons would result in the occupation of strongly antibonding levels. The lowest CVE limit is probably much lower, owing to the fact that the lowest predicted and observed (so far) values for the noncentered $M_8(\mu_4\text{-}E)_6L_8$ species are 76[11] and 99,[6] respectively.

Conclusion

Although only one example of main-group atom-centered hexacapped cubic clusters of the type $M_8(\mu_8\text{-}E')(\mu_4\text{-}E)_6L_8$ is known so far, namely **1a**,[16] DFT calculations that we carried out indicate that there is no reason for this kind of compound to be unstable. It is therefore very likely that other members of this family will be characterized in the future. The major challenge for their synthesis appears to be the accomplishment of the right combinations of the various M, E, E′, and L building blocks in such a way that they would fit with an allowed CVE count and a reasonable ionic charge (if any).[18]

As for their metal-centered parents,[12] there are several "magic" electron numbers susceptible to satisfy the closed-shell requirement for stable $M_8(\mu_8\text{-}E')(\mu_4\text{-}E)_6L_8$ molecules. The most probable electron counts are 120 and 122. The former is favored when E′ is an early main-group element while the latter is favored when E′ is a late main-group element. These two CVE counts are the corresponding values of the most commonly encountered 120-CVE number in noncentered $M_8(\mu_4\text{-}E)_6L_8$ clusters.[5][11] They imply substantial M−M bonding. In the particular case where the capping ligand E is a bare heavy main-group atom, these two closed-shell electron counts diminish to 116 and 118, respectively. In the case of stronger M−M overlap, the highest level of the d-manifold, of t_{2g} symmetry, can become unavailable, favoring the 114-CVE count. Conversely, weak M−M overlap allows the occupation of the lowest M−E antibonding level, of t_{1u} symmetry, leading to the closed-shell count of 128 CVEs. It is likely that this value constitutes the upper limit of the allowed CVE range, since adding more electrons would result in the occupation of strongly antibonding levels. As for their noncentered and metal-centered relatives, there must be a continuum within this allowed range of electron counts for $M_8(\mu_8\text{-}E')(\mu_4\text{-}E)_6L_8$ species.[6][8] Most of these electron counts should correspond to open-shell configurations or small HOMO/LUMO gaps associated with the absence of, or only weak, Jahn−Teller instability, as suggested by the calculations we performed on some of them. A similar stability with respect to the capped cubic architecture was found for the noncentered and metal-centered relatives.[5,11−13] The lowest limit of the allowed CVE range is probably much lower than the closed-shell 114 count, owing to the fact that the lowest predicted and (so far) observed values for the noncentered $M_8(\mu_4\text{-}E)_6L_8$ species are 76[11] and 99,[6] respectively. Assuming orbital interactions as depicted in Figure 1a, the lowest hypothetical limit is also 76 CVE. Such a value should be approached with M = Fe or earlier transition metals.

Regardless of the real limits of the allowed range of electron counts within the whole $M_8(\mu_8\text{-}E')(\mu_4\text{-}E)_6L_8$ series of compounds, its large width suggests that one particular member of this family should have by itself a significant range of allowed CVE counts, i.e. should behave as an electron reservoir and/or sink. For example, compound **1a** is a very good electron donor, owing to the ionization potential calculated for model **1b** (4.8 eV). This value is close to that of the famous 19-electron electron-reservoir $(\eta^5\text{-}C_5H_5)Fe(\eta^6\text{-}C_6Me_6)$ complex.[19] It is likely that, as for $(\eta^5\text{-}C_5H_5)Fe(\eta^6\text{-}C_6Me_6)$, the kinetic stability of **1a** is partly due to the protection of the reactive centers by bulky ligands.

Experimental Section

Density functional calculations were carried out on $Ni_8(\mu_8\text{-}As)(\mu_4\text{-}As)_6(PH_3)_8$ and related species using the Amsterdam Density Functional (ADF) program.[20] Becke exchange[21] and Perdew correlation[22] nonlocal gradient corrections were included in the local density approximation.[23][24] The geometry optimization was based on the method developed by Versluis and Ziegler.[25] The Slater-type basis was of triple-ζ quality. The Ni, Co, and Cu (1s−3p); C and O (1s); Si, P, and S (1s−2p); Ge, As, and Se (1s−3d) cores were kept frozen.[26] Single-ζ 4p polarization functions were included in the Ni, Co, and Cu valence sets, as well as a single-ζ 3d one in the C and O valence sets, a single-ζ 4d one in the Si, P, S, Ge, As, and Se valence sets and a single-ζ 2p one in the H basis set. Test calculations carried out with f polarization functions on Ni and As atoms give results similar to those carried out without f polarization functions.

Acknowledgments

Exchanges between the groups in Amsterdam and Rennes have been made possible through a European Human Capital and Mobility Network Grant (ERBCHRXCT-930156). J.-F. H. and J.-Y. S. thank the Centre de Ressources Informatiques (CRI) of Rennes and the Institut de Développement et de Ressources en Informatique Scientifique du Centre National de la Recherche Scientifique (IDRIS-CNRS) of Orsay for computing facilities. We are grateful to Prof. D. Fenske (Karlsruhe) for helpful discussions.

[1] D. M. P. Mingos, D. J. Wales, *Introduction to Cluster Chemistry*, Prentice-Hall, Englewood Cliffs, New Jersey, **1990**.
[2] *Clusters and Colloids, From Theory to Applications* (Ed.: G. Schmid), VCH, Weinheim, **1994**.
[3] C. Mealli, J. A. Lopez, Y. Sun, M. J. Calhorda, *Inorg. Chim. Acta* **1993**, *213*, 199.
[4] Z. Lin, M.-F. Fan, *Struct. Bonding* **1997**, *87*, 35.
[5] J.-F. Halet, J.-Y. Saillard, *Struct. Bonding* **1997**, *87*, 81.
[6] [6a] L. D. Lower, L. F. Dahl, *J. Am. Chem. Soc.* **1976**, *98*, 5046. – [6b] D. Fenske, R. Basoglu, J. Hachgenei, F. Rogel, *Angew. Chem. Int. Ed. Engl.* **1984**, *23*, 160. – [6c] D. Fenske, J. Magull, *Z. Naturforsch.* **1990**, *45b*, 121. – [6d] D. Fenske, H. Krautscheid, M. Müller, *Angew. Chem. Int. Ed. Engl.* **1992**, *31*, 321. – [6e] D. Fenske, J. Hachgenei, J. Ohmer, *Angew. Chem. Int. Ed. Engl.* **1985**, *24*, 706. – [6f] D. Fenske, J. Ohmer, J. Hachgenei, K. Merzweiler, *Angew. Chem. Int. Ed. Engl.* **1988**, *27*, 1277. – [6g] D. Fenske, J. Hachgenei, F. Rogel, *Angew. Chem. Int. Ed. Engl.* **1984**, *23*, 982. – [6h] G. Christou, K. S. Hagen, J. K. Bashkin, R. H. Holm, *Inorg. Chem.* **1985**, *24*, 1010. – [6i] S. Pohl, U. Opitz, *Angew. Chem. Int. Ed. Engl.* **1993**, *32*, 863. – [6j] S. Pohl, W. Barklage, W. Saak, U. Opitz, *J. Chem. Soc., Chem. Commun.* **1993**, 1251. – [6k] C. Junghans, W. Saak, S. Pohl, *J. Chem. Soc., Chem. Commun.* **1994**, 2327. – [6l] S. Pohl, W. Saak, *Angew. Chem. Int. Ed. Engl.* **1984**, *23*, 907. – [6m] A. M. Arif, R. A. Jones, D. E. Heaton, C. M. Nunn, S. T. Scwab, *Inorg. Chem.* **1988**, *27*, 254.
[7] [7a] L. E. McCandlish, E. C. Bissell, D. Coucouvanis, J. P. Fackler, K. Knox, *J. Am. Chem. Soc.* **1968**, *90*, 7357. – [7b] F. J. Hollander, D. Coucouvanis, *J. Am. Chem. Soc.* **1974**, *96*, 5646. – [7c] A. Avdeef, J. P. Fackler, *Inorg. Chem.* **1978**, *17*, 2182.
[8] [8a] J. G. Brennan, T. Siegrist, S. Stuczynski, M. L. Steigerwald, *J. Am. Chem. Soc.* **1989**, *111*, 9240. – [8b] D. Fenske, H. Fleischer, C. Persau, *Angew. Chem. Int. Ed. Engl.* **1989**, *28*, 1665. – [8c] D. Fenske, C. Persau, *Z. Anorg. Allg. Chem.* **1991**, *593*, 61. – [8d] J. P. Zebrowski, R. K. Hayashi, A. Bjarnason, L. F. Dahl, *J. Am. Chem. Soc.* **1992**, *114*, 3121. – [8e] D. Fenske, J. Ohmer, K. Merzweiler, *Angew. Chem. Int. Ed. Engl.* **1988**, *27*, 1512.
[9] K. H. Whitmire, J. R. Eveland, *J. Chem. Soc., Chem. Commun.* **1994**, 1335.
[10] [10a] D. Wu, J. Q. Huang, Y. Lin, J. L. Huang, *Sci. Sin. Ser. B (Engl. Ed.)* **1988**, *31*, 800. – [10b] Z. H. Huang, S. F. Lu, J. Q. Huang, D. M. Wu, J. L. Huang, *Jiegou Huaxue* **1991**, *10*, 213. – [10c] I. Haiduc, D. B. Sowerby, S. F. Lu, *Polyhedron* **1995**, *14*, 3389. – [10d] C. W. Liu, T. Stubbs, R. J. Staples, J. P. Fackler, *J. Am. Chem. Soc.* **1995**, *117*, 9778. – [10e] C. W. Liu, H.-S. Chen, J.-C. Wang, T.-C. Keng, *J. Chem. Soc., Chem. Commun.* **1998**, 1831.
[11] E. Furet, A. Le Beuze, J.-F. Halet, J.-Y. Saillard, *J. Am. Chem. Soc.* **1994**, *116*, 274. See also: N. Rösch, L. Ackermann, G. Pacchioni, *Inorg. Chem.* **1993**, *32*, 2963.
[12] E. Furet, A. Le Beuze, J.-F. Halet, J.-Y. Saillard, *J. Am. Chem. Soc.* **1995**, *117*, 4936.
[13] [13a] B. Zouchoune, F. Ogliaro, J.-F. Halet, J.-Y. Saillard, J. R. Eveland, K. H. Whitmire, *Inorg. Chem.* **1998**, *37*, 5, 865. – [13b] R. Gautier, J.-F. Halet, J.-Y. Saillard, *Eur. J. Inorg. Chem.* **1999**, 673.
[14] R. A. Wheeler, *J. Am. Chem. Soc.* **1990**, *112*, 8737; *J. Am. Chem. Soc.* **1991**, *113*, 4046.
[15] [15a] D. M. P. Mingos, *J. Chem. Soc., Chem. Commun.* **1985**, 1353. – [15b] D. M. P. Mingos, Z. Lin, *J. Chem. Soc., Dalton Trans.* **1998**, 1657.
[16] [16a] D. Fenske, K. Vogt, unpublished results. – [16b] K. Vogt, Ph.D. Dissertation, University of Karlsruhe, Germany, **1994**.
[17] F. Ogliaro, S. Cordier, J.-F. Halet, C. Perrin, J.-Y. Saillard, M. Sergent, *Inorg. Chem.* **1998**, *37*, 6199.
[18] Unlike for most of the empty and metal-centered capped cubic clusters,[11–13] we found that extended Hückel calculations lead to conclusions that, even at a qualitative level, strongly disagree with DFT calculations. In particular, the a_{1g} interaction (see Figure 1) is always found to be very strong at the extended Hückel level, whatever is the nature of E′. In addition, the e_g effect caused by E when it is a bare atom appears to be systematically overestimated when compared to the DFT results. As a result, most of the favored electron counts as predicted by extended Hückel theory are likely to be unrealistic.
[19] D. Astruc, *Electron Transfer and Radical Processes in Transition Metal Chemistry*, VCH Publishers, **1995**.
[20] [20a] E. J. Baerends, D. E. Ellis, P. Ros, *Chem. Phys.* **1973**, *2*, 41. – [20b] *Amsterdam Density Functional (ADF) program, version 2.0.1*, Vrije Universiteit, Amsterdam, Netherlands, **1996**.
[21] A. D. Becke, *Phys. Rev. A* **1988**, *38*, 3098.
[22] J. P. Perdew, *Phys. Rev. B* **1986**, *33*, 8822; J. P. Perdew, *Phys. Rev. B* **1986**, *34*, 7046.
[23] S. H. Vosko, L. Wilk. M. Nusair, *Can. J. Phys.* **1980**, *58*, 1200.
[24] H. Stoll, E. Golka, E. Preuss, *Theoret. Chim. Acta* **1980**, *29*, 55.
[25] L. Versluis, T. Ziegler, *J. Chem. Phys.* **1988**, *88*, 322.
[26] [26a] E. J. Baerends, P. Ros, *Chem. Phys.* **1975**, *8*, 41. – [26b] E. J. Baerends, P. Ros, *Int. J. Quantum. Chem.* **1978**, *S12*, 169, and references cited therein.

Received December 18,1998
[I98448]